Available online at www.sciencedirect.com
ScienceDirect
Geochimica et Cosmochimica Acta 73 (2009) 2674–2691
Geochimica et Cosmochimica Acta
www.elsevier.com/locate/gca

The iron–nickel–phosphorus system: Effects on the distribution of trace elements during the evolution of iron meteorites

Catherine M. Corrigan [a,*], Nancy L. Chabot [b], Timothy J. McCoy [a], William F. McDonough [c], Heather C. Watson [d], Sarah A. Saslow [e], Richard D. Ash [c]

[a] *Department of Mineral Sciences, National Museum of Natural History Smithsonian Institution, 10th Street and Constitution Ave. NW, Washington, DC 20560-0119, USA*
[b] *Johns Hopkins University Applied Physics Laboratory, 11100 Johns Hopkins Road, Laurel, MD 20723, USA*
[c] *Department of Geology, University of Maryland, College Park, MD 20742, USA*
[d] *Lawrence Livermore National Laboratory, 7000 East Ave. L-206, Livermore, CA 94550, USA*
[e] *University of Maryland, College Park, MD 20742, USA*

Received 18 March 2008; accepted in revised form 25 November 2008; available online 8 February 2009

Abstract

To better understand the partitioning behavior of elements during the formation and evolution of iron meteorites, two sets of experiments were conducted at 1 atm in the Fe–Ni–P system. The first set examined the effect of P on solid metal/liquid metal partitioning behavior of 22 elements, while the other set explored the effect of the crystal structures of body-centered cubic (α)- and face-centered cubic (γ)-solid Fe alloys on partitioning behavior. Overall, the effect of P on the partition coefficients for the majority of the elements was minimal. As, Au, Ga, Ge, Ir, Os, Pt, Re, and Sb showed slightly increasing partition coefficients with increasing P-content of the metallic liquid. Co, Cu, Pd, and Sn showed constant partition coefficients. Rh, Ru, W, and Mo showed phosphorophile (P-loving) tendencies. Parameterization models were applied to solid metal/liquid metal results for 12 elements. As, Au, Pt, and Re failed to match previous parameterization models, requiring the determination of separate parameters for the Fe–Ni–S and Fe–Ni–P systems.

Experiments with coexisting α and γ Fe alloy solids produced partitioning ratios close to unity, indicating that an α versus γ Fe alloy crystal structure has only a minor influence on the partitioning behaviors of the trace element studied. A simple relationship between an element's natural crystal structure and its α/γ partitioning ratio was not observed. If an iron meteorite crystallizes from a single metallic liquid that contains both S and P, the effect of P on the distribution of elements between the crystallizing solids and the residual liquid will be minor in comparison to the effect of S. This indicates that to a first order, fractional crystallization models of the Fe–Ni–S–P system that do not take into account P are appropriate for interpreting the evolution of iron meteorites if the effects of S are appropriately included in the effort.
Published by Elsevier Ltd.

1. INTRODUCTION

Iron meteorites formed by the crystallization of metallic liquids on numerous asteroid-sized parent bodies. Some iron meteorites likely represent the central metallic cores of subsequently disrupted asteroids while other iron meteorites may have solidified in large molten metallic pools not located in the center of an asteroid (e.g. review by Haack and McCoy, 2003). Whatever the crystallization environment and method, the composition of the metallic liquid, especially the concentrations of light elements such as S, C, and P in the liquid, are believed to have played a significant role in the crystallization and evolution of iron meteorites.

During crystallization, trace elements partition between the crystallizing solid metal and the residual liquid metal, and experimental studies have demonstrated that the con-

* Corresponding author.
E-mail address: corriganc@si.edu (C.M. Corrigan).

0016-7037/$ - see front matter Published by Elsevier Ltd.
doi:10.1016/j.gca.2008.11.045

centrations of the light elements S, C, and P, in the metallic liquid can cause significant variations in the partitioning behaviors of trace elements (e.g. Willis and Goldstein, 1982; Jones and Drake, 1983; Chabot et al., 2003, 2006). Additionally, as crystallization of a metallic melt proceeds, the light elements are excluded from the solid metal and enriched in the liquid metal, enhancing their effects on the trace element partitioning behaviors and, in turn, on the compositions of crystallizing iron meteorites. Some iron meteorites groups (IIAB, IIIAB, IVA, and IVB) are believed to have evolved in the Fe–Ni–S–P system (e.g. Jones and Drake, 1983; Ulff-Møller, 1998), and in this system, there is a large liquid immiscibility field (Raghavan, 1988). If liquid immiscibility was encountered during the crystallization of iron meteorites, understanding both the effects of S and P on the trace element partitioning behavior would be crucial to understanding how elements would distribute themselves between the two immiscible liquids that formed, one of which would be S-rich and the other P-rich. These light elements also form a variety of inclusions common in iron meteorites, such as sulfides, carbides, graphite, and phosphides (e.g. Buchwald, 1975). During solidification, P, in particular, plays a significant role in the formation of the metallographic structure in iron meteorites, including the development of the Widmanstätten pattern (Yang and Goldstein, 2005).

Many experimental studies have focused on determining the effect of S on solid metal/liquid metal partitioning behavior. References for these numerous studies can be found in Jones and Malvin (1990) and Chabot et al. (2003). Some highly siderophile (metal-loving) elements, such as Ir, exhibit as much as a three order of magnitude change in their solid metal/liquid metal partition coefficient as the S-content increases from the S-free system to a composition of 31 wt% S at the Fe–FeS eutectic. In contrast, other elements, such as Cr, behave as chalcophile (S-loving) elements and their solid metal/liquid metal partition coefficients decrease with increasing S in the metallic liquid. Chabot et al. (2006) recently completed a multi-element systematic study of solid metal/liquid metal partitioning in the Fe–Ni–C system. That study found that some elements, such as Re and W, behave as anthracophile (C-loving) elements, with decreasing solid metal/liquid metal partition coefficients with increasing C content of the system; this behavior is opposite to the effect of S on Re and W partitioning, where the partition coefficients increase significantly with increasing amounts of S in the metallic liquid. These few examples illustrate the fact that trace elements are affected differently by different light elements.

Though P is acknowledged as an important light element in iron meteorite systems, experimental determinations of the effects of P on trace element face-centered cubic (γ-phase solid metal/liquid metal partitioning behavior are limited. Narayan and Goldstein (1982) conducted five experiments in the Fe–Ni–P system, examining the solid metal/liquid metal partitioning behavior of Ge. Willis and Goldstein (1982) conducted six similar experiments, two each with the trace elements Au, Ga, and Ir. Malvin et al. (1986) reported six experiments in the Fe–Ni–P system, two each for the trace elements Au, Ge, and Ir. Jones and Malvin (1990) listed three new solid metal/liquid metal P-bearing experiments, one each for Au, Ge, and Ir. The results of these previous solid metal/liquid metal Fe–Ni–P experimental studies are detailed in the Appendix and listed in Table A1. Experimental data from Sellamuthu and Goldstein (1983, 1984, 1985) were not directly compared to data produced here, as their experiments were based on disequilibrium crystallization in an attempt to simulate fractional crystallization, while ours are static equilibrium experiments. No other experimental data exist for trace element partitioning between γ-phase solid metal and liquid metal in the Fe–Ni–P system. Previous studies were hindered, however, by the necessity to physical separate solid and liquid metal and then analyze each independently (sometimes doped with wt% levels of a small number of elements). The LA-ICP-MS technique has allowed this study to be possible, as we do not have to separate the metallic phases for analysis, and can analyze multiple elements, at levels comparable to those found in iron meteorites, simultaneously. The validity of this technique being used for experiments in the Fe system was discussed in depth in Chabot et al. (2003). These authors showed that experiments doped with multiple trace elements at ppm levels yielded partition coefficients that agreed with those determined in systems doped with only a single element. Thus, there are no significant cross-element effects on partitioning among the trace elements.

In this work, we present the results of solid metal/liquid metal partitioning experiments in the Fe–Ni–P system conducted for a large suite of trace elements relevant to the crystallization of iron meteorites. We also present experiments that examine the partitioning behavior between different solid metal phases in the Fe–Ni–P system, the results of which are appropriate for comparison to measured kamacite/taenite partition coefficients in iron meteorites. This new experimental data set provides insight into the effect of P on trace element partitioning in the Fe–Ni–P system and is the first such data for 17 of the trace elements studied.

2. EXPERIMENTAL AND ANALYTICAL METHODS

Fe–Ni–P experiments were conducted in one-atmosphere Deltech vertical tube furnaces at the Smithsonian Institution, NASA's Johnson Space Center, and Johns Hopkins University Applied Physics Lab. All experiments were run using methods similar to those used in previous studies involving solid metal/liquid metal studies (Jones and Drake, 1983; Chabot et al., 2003). Starting powders were mixtures of the major components of Fe, Ni, and P and a mixture of 22 trace elements doped at ~100 ppm each. These trace elements were in the form of high purity, commercially purchased powders, and included Ag, As, Au, Bi, Co, Cr, Cu, Ga, Ge, Ir, Mo, Os, Pb, Pd, Pt, Re, Rh, Ru, Sb, Sn, W, and Zn. Nickel was present at ~8–10 wt% and the P-content of the starting powder varied with consideration of the Fe–P phase diagram (Doan and Goldstein, 1970).

For each experiment, ~0.2–0.3 g of the starting powder was contained in an evacuated silica tube. The majority of

the powders were placed in an alumina crucible within the evacuated silica tube while four experiments simply inserted the starting powder directly into the silica tube (runs #CC1, CC2, CC4, and CC5); all of the runs produced consistent partitioning behavior, suggesting that the presence of an alumina crucible was not necessary for these experiments, a conclusion also demonstrated by Chabot et al. (2007). These silica tubes were hung within the Deltech furnaces for lengths of time varying from 14 h to 7 days. The length of time varied inversely with the temperature, with shorter durations corresponding to runs at higher temperatures. Experimental temperatures ranged from 1100 to 1500 °C, increasing in 50 °C increments. In addition, an 1125 °C run was conducted to better constrain the partitioning behavior at the low end of the temperature scale.

Upon removal from the furnace, still-sealed silica tubes were immediately submerged in cold water. Experimental charges were then released from the alumina crucibles (if contained in one), sliced, made into a polished section, and examined. The original goal of the experiments was to create experimental run products that contained coexisting equilibrium solid metal and liquid metal, to determine the partitioning behavior of trace elements between these two phases as related to the crystallization of iron meteorites. During the solidification of iron meteorites, which occurs in a low-P, Fe–Ni system, solid metal with a face-centered cubic structure (γ) crystallizes from the metallic liquid. As the iron meteorite cools, the γ-phase mineral taenite transforms to body-centered cubic α-phase kamacite, creating the distinctive Widmanstätten pattern present in many iron meteorites (e.g. Yang and Goldstein, 2005). In the Fe–P system, the solid metal that coexists with liquid metal has the α structure; however, the addition of Ni stabilizes the formation of the γ-phase solid metal coexisting with liquid metal in the Fe–Ni–P system (Doan and Goldstein, 1970). Because the goal of this work was to examine the behavior of elements during the crystallization of iron meteorites, Ni was added to the experiments to produce run products that contained coexisting γ-phase solid metal and liquid metal. A value of 8 wt% Ni was selected to match the average Ni concentration of a range of iron meteorite groups, including that of the IIIAB and IVA groups (Wasson, 1999; Wasson and Richardson, 2001).

At temperatures $\geqslant$1200 °C, experiments with 8 wt% Ni produced the desired two phases of γ-phase solid metal and liquid metal. In contrast, experiments run with 8 wt% Ni at 1150 °C produced results that lay within the α-γ-liquid three-phase field, and an experiment at 1100 °C produced a result within the α-liquid field. In order to produce a comprehensive set of experiments which all fell in the γ-liquid field, additional experiments between 1100 and 1200 °C were conducted using 10 wt% Ni. A 1500 °C experiment was composed of only liquid metal. Altogether, nine experiments that consisted of two-phases of γ-solid metal and liquid metal were completed, and the conditions of these experiments are given in Table 1.

However, examining partitioning between coexisting α-phase and γ-phase solid metal is also of interest to iron meteorites, which contain both kamacite and taenite. We thus decided to take advantage of the α-γ-liquid three-phase field in the Fe–Ni–P ternary system to determine how trace elements partition between these two solid metal phases. This three-phase field is small, with bulk compositions varying from about 2 to 13 wt% P and 6 to 10 wt% Ni over the temperature range from about 1000 to 1150 °C (Doan and Goldstein, 1970). Five experiments were conducted between 1100 and 1150 °C that produced coexisting α-phase, γ-phase, and liquid metal, and details for these runs are provided in Table 2.

Each experiment was imaged and analyzed to determine major element compositions (Fe, Ni, and P) using the JEOL JXA 8900R electron microprobe at the Smithsonian Institution or the JEOL 8900L at the Carnegie Institution of Washington. The electron microprobe analysis was conducted using beam conditions of 15–20 kV, 20–30 nA, counting times of 30 s, and either a beam rastered over a 20 μm by 20 μm area or a defocused 20 μm diameter beam. For each phase, 5–99 individual measurements were averaged to determine the bulk composition, with the number of analyses depending on the beam size and quench texture of the phase being measured. This analytical approach has been demonstrated to determine accurately the bulk composition of the quenched metallic liquid when multiple measurements are averaged (Chabot and Drake, 1997). Errors were calculated as twice the standard error of the mean.

Back-scattered electron (BSE) images of two of the γ-solid metal/liquid metal runs are shown in Fig. 1. The runs exhibit clear separation of the solid metal and liquid metal phases. The solid metal is homogeneous in composition, while the liquid metal was a single-phase liquid at run conditions but, upon removal from the furnace, quenched to a dendritic texture. As discussed in more detail later, results of the partitioning analyses are in good agreement with the limited previous P-bearing solid metal/liquid metal data, suggesting that equilibrium was reached in the experiments. A BSE image of an experiment with three-phases at run temperature, an $\alpha-\gamma$-liquid experiment, is shown in Fig. 2, with the contrast enhanced to show the two different solid metal phases. Solid metal was identified as being either α or γ at the temperature of the experiment based on their easily distinguished Ni and P contents in this system; consistent with the Fe–Ni–P phase diagram at about 1100 °C (Doan and Goldstein, 1970), in our experiments, γ-solid metal phase has a composition of about 1.1 wt% P and 8.0 wt% Ni, while the α-solid metal phase has 2.1 wt% P and 6.5 wt% Ni. Both of the solid metal phases were homogenous, while the P-rich metallic liquid did not quench to a single phase but rather produced a typical dendritic texture.

Each experimental run product was analyzed for trace element concentrations by laser ablation inductively coupled plasma mass spectrometry (ICP-MS) at the University of Maryland. In-situ analyses were carried out using a single-collector ICP-MS (Element 2, Thermo Electron Corp.) coupled to a laser ablation system with an output wave-

Table 1
Compositions of solid metal and liquid metal phases.

Run #	P24	P20	P22	P25	P11	P4	P1J	P5J	P6J
Temperature (°C)	1100	1125	1150	1200	1250	1300	1350	1400	1450
Duration (h)	168	168	168	168	168	96	93	14	14
Bulk (wt%)									
Fe	82.5	82.5	83.3	83.3	86.6	86.6	89.3	89.3	89.3
Ni	10.0	10.0	10.0	10.0	8.0	8.0	8.0	8.0	8.0
P	7.31	7.31	6.42	6.42	5.21	5.21	2.50	2.50	2.50
Traces	0.21	0.21	0.21	0.21	0.21	0.21	0.21	0.21	0.21
Solid metal									
Fe (wt%)	90.0 ± 0.1	90.2 ± 0.1	90.7 ± 0.1	90.0 ± 0.1	91.3 ± 0.4	91.3 ± 0.2	90.9 ± 0.1	91.4 ± 0.5	90.9 ± 0.2
Ni (wt%)	8.4 ± 0.03	8.4 ± 0.02	7.7 ± 0.02	8.9 ± 0.01	7.6 ± 0.04	7.4 ± 0.04	7.8 ± 0.04	7.5 ± 0.03	7.3 ± 0.04
P (wt%)	1.1 ± 0.01	1.1 ± 0.01	1.0 ± 0.004	0.9 ± 0.004	0.8 ± 0.02	0.6 ± 0.02	0.5 ± 0.01	0.4 ± 0.01	0.3 ± ± 0.01
Ag (ppm)	15 ± 1	10 ± 0.1	11 ± 0.3	19 ± 1	18 ± 0.4	13 ± 2			30 ± 1
As (ppm)	79 ± 3	66 ± 1	39 ± 1	38 ± 1	75 ± 2	46 ± 1	72 ± 1	57 ± 1	70 ± 1
Au (ppm)	74 ± 2	78 ± 1	94 ± 3	83 ± 2	117 ± 5	82 ± 1	92 ± 1	75 ± 1	89 ± 1
Bi (ppm)	0.3 ± 0.02	0.3 ± 0.02	0.3 ± 0.02	1 ± 0.1	1 ± 0.1				2 ± 0.1
Co (ppm)	89 ± 1	88 ± 1	129 ± 2	119 ± 2	191 ± 4	163 ± 0.8	162 ± 2	181 ± 3	220 ± 2
Cr (ppm)				9 ± 0.3	23 ± 1	28 ± 1	28 ± 1	61 ± 3	76 ± 2
Cu (ppm)	352 ± 5	359 ± 7	347 ± 2		504 ± 6	385 ± 4	381 ± 8	460 ± 15	450 ± 6
Ga (ppm)	11 ± 0.1	10 ± 0.2	10 ± 0.3	12 ± 0.2	18 ± 1	17 ± 0.2	19 ± 1	16 ± 1	19 ± 1
Ge (ppm)	162 ± 4	155 ± 3	93 ± 1	97 ± 1	196 ± 4	143 ± 3	134 ± 2	129 ± 4	148 ± 4
Ir (ppm)	170 ± 3	149 ± 4		113 ± 3	374 ± 13	423 ± 8		347 ± 11	450 ± 11
Mo (ppm)	41 ± 1	36 ± 1	40 ± 1	44 ± 1	88 ± 2	67 ± 1	108 ± 1	103 ± 2	120 ± 3
Os (ppm)	208 ± 5	187 ± 4		175 ± 6	492 ± 10	577 ± 17		370 ± 12	503 ± 17
Pb (ppm)	1 ± 0.02	1 ± 0.04	1 ± .03	1 ± 0.1	3 ± 0.1				2 ± 0.1
Pd (ppm)	52 ± 1	56 ± 2	41 ± 1	42 ± 1	105 ± 3	91 ± 6	58 ± 1	61 ± 2	67 ± 1
Pt (ppm)	227 ± 4	258 ± 8	211 ± 12	247 ± 8	261 ± 10	210 ± 4	141 ± 2	161 ± 4	195 ± 6
Re (ppm)	163 ± 4	149 ± 4	94 ± 6	131 ± 3	222 ± 6	228 ± 3		196 ± 5	251 ± 2
Rh (ppm)	90 ± 2	114 ± 3	108 ± 2	91 ± 2	202 ± 5	119 ± 1	108 ± 1	154 ± 5	116 ± 2
Ru (ppm)	87 ± 2	81 ± 2	73 ± 2	88 ± 2	216 ± 5	106 ± 3	230 ± 2	204 ± 4	224 ± 8
Sb (ppm)	35 ± 1	35 ± 1	27 ± 1	24 ± 1	42 ± 1	27 ± 2	41 ± 1	29 ± 1	38 ± 1
Sn (ppm)	33 ± 1	34 ± 1	23 ± 1	26 ± 1	44 ± 1	29 ± 2	36 ± 1	33 ± 2	42 ± 1
W (ppm)	77 ± 2	81 ± 3	117 ± 3	100 ± 3	136 ± 4	104 ± 1	91 ± 1	122 ± 4	104 ± 2
Liquid metal									
Fe (wt%)	81.5 ± 1.1	80.7 ± 1.0	82.9 ± 1.0	82.1 ± 0.9	83.7 ± 1.7	85.4 ± 1.9	86.0 ± 0.8	87.4 ± 1.6	87.5 ± 0.9
Ni (wt%)	9.6 ± 0.3	9.7 ± 0.3	8.9 ± 0.4	9.8 ± 0.2	8.5 ± 0.3	8.4 ± 0.4	8.7 ± 0.2	8.4 ± 0.3	8.3 ± 0.2
P (wt%)	8.8 ± 1.1	9.3 ± 1.0	7.9 ± 0.9	7.8 ± 0.9	7.9 ± 1.8	6.0 ± 1.6	4.9 ± 0.8	3.7 ± 1.3	3.1 ± 0.8
Ag (ppm)	130 ± 12	89 ± 7	94 ± 11	170 ± 8	82 ± 6	64 ± 13		1 ± 0.1	166 ± 19
As (ppm)	121 ± 4	97 ± 2	72 ± 3	82 ± 3	132 ± 4	97 ± 3	182 ± 13	155 ± 5	192 ± 5
Au (ppm)	79 ± 2	81 ± 3	111 ± 6	107 ± 2	135 ± 2	105 ± 2	143 ± 4	136 ± 4	156 ± 3
Bi (ppm)	54 ± 7	46 ± 5	41 ± 7	108 ± 8	78 ± 8				115 ± 19
Co (ppm)	84 ± 1	83 ± 1	125 ± 3	113 ± 1	150 ± 5	125 ± 3	123 ± 3	155 ± 4	172 ± 1
Cr (ppm)	3 ± 0.03			14 ± 1	22 ± 1	28 ± 4	32 ± 3.0	53 ± 3	59 ± 4
Cu (ppm)	341 ± 9	354 ± 6	383 ± 7		421 ± 3	331 ± 3	343 ± 6	466 ± 7	451 ± 12
Ga (ppm)	4 ± 1	4 ± 0.4	4 ± 0.4	6 ± 0.3	9 ± 0.2	10 ± 0.2	14 ± 1	13 ± 1	18 ± 1
Ge (ppm)	67 ± 7	65 ± 4	44 ± 3	52 ± 2	105 ± 2	88 ± 2	93 ± 7	117 ± 3	126 ± 2
Ir (ppm)	20 ± 4	19 ± 2		17 ± 1	59 ± 1	87 ± 5		107 ± 4	112 ± 13
Mo (ppm)	135 ± 5	118 ± 3	120 ± 5	119 ± 3	175 ± 4	115 ± 5	167 ± 7	159 ± 7	176 ± 5
Os (ppm)	24 ± 5	23 ± 2		23 ± 2	65 ± 1	100 ± 9		94 ± 5	102 ± 14
Pb (ppm)	50 ± 8	53 ± 4	71 ± 13	115 ± 15	96 ± 9				72 ± 9
Pd (ppm)	80 ± 1	83 ± 2	69 ± 4	71 ± 3	119 ± 4	95 ± 4	82 ± 2	90 ± 3	97 ± 1
Pt (ppm)	51 ± 8	58 ± 4	53 ± 8	68 ± 4	71 ± 1	73 ± 2	47 ± 9	91 ± 4	94 ± 6
Re (ppm)	34 ± 5	32 ± 2	21 ± 3	30 ± 2	47 ± 0.4	55 ± 3		69 ± 3	70 ± 7
Rh (ppm)	84 ± 1	104 ± 2	100 ± 3	81 ± 1	156 ± 2	89 ± 1	75 ± 4	128 ± 4	86 ± 2
Ru (ppm)	65 ± 2	60 ± 2	54 ± 2	62 ± 1	125 ± 3	68 ± 2	119 ± 13	122 ± 1	117 ± 8
Sb (ppm)	123 ± 6	115 ± 4	102 ± 8	106 ± 7	131 ± 9	93 ± 4	204 ± 34	141 ± 7	200 ± 14
Sn (ppm)	145 ± 7	136 ± 6	108 ± 9	135 ± 12	164 ± 8	110 ± 4	194 ± 24	166 ± 10	233 ± 17
W (ppm)	81 ± 3	81 ± 2	117 ± 4	95 ± 1	103 ± 1	74 ± 1	61 ± 7	97 ± 4	73 ± 4

Measurements of Fe, Ni, and P were made using the electron microprobe. All other elements were analyzed by LA-ICP-MS. Errors are $\pm 2\sigma$.

Table 2
Composition of three-phase experiments with α-solid metal, γ-solid metal, and liquid metal.

Run #	CC1	CC2	CC4	CC5	P1150
Temperature (°C)	1104	1102	1114	1118	1150
Duration (days)	9	7	8	6	7
Bulk (wt%)					
Fe	88.5	86.0	88.5	86.0	
Ni	7.5	8.0	7.5	8.0	
P	4.0	6.0	4.0	6.0	
Traces	0.5	0.5	0.5	0.5	
α-*Solid*					
Fe (wt%)	91.7 ± 0.9	91.2 ± 0.7	91.0 ± 1.0	90.3 ± 0.8	91.0 ± 0.3
Ni (wt%)	6.6 ± 0.1	6.6 ± 0.1	6.6 ± 0.1	6.3 ± 0.1	6.3 ± 0.1
P (wt%)	2.1 ± 0.1	2.2 ± 0.1	2.1 ± 0.1	2.1 ± 0.1	2.1 ± 0.1
Ag (ppm)			19 ± 6	12 ± 1	16 ± 2
As (ppm)	180 ± 20	141 ± 12	160 ± 20	132 ± 5	41 ± 5
Au (ppm)	250 ± 30	240 ± 20	330 ± 30	360 ± 30	66 ± 5
Bi (ppm)			1.3 ± 0.2	1.1 ± 0.2	0.75 ± 0.12
Co (ppm)	411 ± 16	392 ± 6	360 ± 20	390 ± 20	124 ± 6
Cr (ppm)	30 ± 7	32 ± 4	3.5 ± 0.8	6.6 ± 0.9	
Cu (ppm)	260 ± 20	290 ± 30	330 ± 30	319 ± 12	250 ± 20
Ga (ppm)	143 ± 7	214 ± 10	156 ± 8	194 ± 11	10.6 ± 0.7
Ge (ppm)	250 ± 20	301 ± 20	250 ± 20	305 ± 12	95 ± 8
Ir (ppm)	270 ± 20	330 ± 20	250 ± 30	350 ± 20	72 ± 3
Mo (ppm)	230 ± 50	147 ± 7	340 ± 50	241 ± 9	73 ± 8
Os (ppm)	210 ± 20	250 ± 20	210 ± 30	296 ± 9	114 ± 14
Pb (ppm)	0.24 ± 0.04	0.36 ± 0.09	3.8 ± 0.5	2.3 ± 0.2	1.5 ± 0.2
Pd (ppm)	200 ± 40	140 ± 20	170 ± 20	154 ± 8	31 ± 5
Pt (ppm)	210 ± 20	220 ± 10	270 ± 30	324 ± 14	170 ± 7
Re (ppm)	220 ± 50	320 ± 50	230 ± 30	350 ± 40	110 ± 5
Rh (ppm)			130 ± 30	101 ± 4	105 ± 7
Ru (ppm)	240 ± 50	203 ± 10	360 ± 70	370 ± 20	66 ± 5
Sb (ppm)	160 ± 20	87 ± 5	290 ± 100	186 ± 9	31 ± 4
Sn (ppm)	180 ± 30	145 ± 8	260 ± 80	186 ± 7	30 ± 4
W (ppm)	190 ± 20	200 ± 20	170 ± 30	194 ± 5	154 ± 6
Zn (ppm)			56 ± 7	64 ± 8	
γ-*Solid*					
Fe (wt%)	91.4 ± 0.7	90.4 ± 0.7	89.9 ± 1.0	90.4 ± 0.7	90.7 ± 0.5
Ni (wt%)	8.2 ± 0.3	8.2 ± 0.2	8.1 ± 0.2	7.8 ± 0.2	7.6 ± 0.1
P (wt%)	1.1 ± 0.1	1.1 ± 0.1	1.1 ± 0.1	1.1 ± 0.1	1.1 ± 0.1
Ag (ppm)			19 ± 2	11 ± 1	16 ± 1
As (ppm)	170 ± 30	137 ± 5	156 ± 9	129 ± 5	44 ± 7
Au (ppm)	300 ± 40	270 ± 30	380 ± 20	380 ± 30	100 ± 20
Bi (ppm)			0.82 ± 0.06	0.74 ± 0.08	0.46 ± 0.06
Co (ppm)	417 ± 13	390 ± 20	350 ± 30	370 ± 20	135 ± 5
Cr (ppm)	25 ± 2	32 ± 11	3.2 ± 0.2	6.0 ± 0.9	
Cu (ppm)	320 ± 20	320 ± 9	360 ± 20	380 ± 30	300 ± 20
Ga (ppm)	170 ± 20	220 ± 20	169 ± 9	198 ± 10	12 ± 1
Ge (ppm)	300 ± 30	340 ± 50	290 ± 10	320 ± 20	120 ± 20
Ir (ppm)	460 ± 40	550 ± 50	400 ± 50	540 ± 30	131 ± 9
Mo (ppm)	150 ± 20	109 ± 6	250 ± 30	173 ± 9	50 ± 2
Os (ppm)	320 ± 30	380 ± 70	300 ± 40	420 ± 20	158 ± 14
Pb (ppm)	0.28 ± 0.14	0.31 ± 0.05	2.2 ± 0.2	1.5 ± 0.1	0.98 ± 0.16
Pd (ppm)	250 ± 40	180 ± 20	224 ± 8	177 ± 8	37 ± 3
Pt (ppm)	340 ± 30	360 ± 30	410 ± 40	500 ± 30	300 ± 20
Re (ppm)	260 ± 30	320 ± 110	260 ± 30	320 ± 30	118 ± 4
Rh (ppm)			163 ± 8	118 ± 6	140 ± 20
Ru (ppm)	280 ± 50	250 ± 20	440 ± 20	410 ± 20	82 ± 4
Sb (ppm)	144 ± 14	82 ± 2	270 ± 40	160 ± 20	29 ± 1
Sn (ppm)	127 ± 14	107 ± 5	200 ± 30	129 ± 8	24 ± 4
W (ppm)	143 ± 7	148 ± 11	130 ± 20	140 ± 5	127 ± 8
Zn (ppm)			59 ± 9	61 ± 9	

Table 2 (*continued*)

Run #	CC1	CC2	CC4	CC5	P1150
Fe (wt%)	81.4 ± 0.7	81.8 ± 0.7	80.7 ± 1.2	81.5 ± 0.9	83.5 ± 1.1
Ni (wt%)	9.5 ± 0.3	9.3 ± 0.2	9.5 ± 0.3	8.9 ± 0.3	8.2 ± 0.5
P (wt%)	8.8 ± 0.4	8.5 ± 0.6	8.9 ± 0.8	8.5 ± 0.6	8.4 ± 1.0
Ag (ppm)			140 ± 20	87 ± 8	170 ± 50
As (ppm)	267 ± 2	238 ± 9	280 ± 7	215 ± 5	77 ± 9
Au (ppm)	325 ± 7	347 ± 8	450 ± 50	460 ± 20	103 ± 14
Bi (ppm)			90 ± 12	50 ± 30	80 ± 20
Co (ppm)	389 ± 9	394 ± 8	345 ± 10	351 ± 2	117 ± 7
Cr (ppm)	45 ± 3	52 ± 6	4.6 ± 0.7	8.3 ± 0.4	1.5 ± 0.2
Cu (ppm)	310 ± 50	340 ± 30	374 ± 7	361 ± 11	267 ± 3
Ga (ppm)	58 ± 5	86 ± 9	78 ± 8	74 ± 10	4.6 ± 0.2
Ge (ppm)	113 ± 4	147 ± 9	145 ± 11	140 ± 20	50 ± 4
Ir (ppm)	55 ± 5	75 ± 9	60 ± 6	70 ± 20	16 ± 2
Mo (ppm)	490 ± 20	410 ± 20	790 ± 70	530 ± 20	139 ± 9
Os (ppm)	36 ± 6	48 ± 4	42 ± 5	48 ± 14	18 ± 1
Pb (ppm)	2.1 ± 0.4	3.8 ± 0.9	110 ± 20		80 ± 20
Pd (ppm)	390 ± 14	350 ± 20	360 ± 20	286 ± 13	55 ± 7
Pt (ppm)	76 ± 5	88 ± 10	106 ± 5	110 ± 20	64 ± 5
Re (ppm)	46 ± 4	78 ± 11	61 ± 2	63 ± 11	23 ± 1
Rh (ppm)			149 ± 2	108 ± 2	122 ± 11
Ru (ppm)	186 ± 5	217 ± 5	315 ± 4	287 ± 8	53 ± 4
Sb (ppm)	487 ± 2	370 ± 20	1000 ± 300	590 ± 20	120 ± 30
Sn (ppm)	530 ± 4	610 ± 60	900 ± 200	570 ± 40	110 ± 40
W (ppm)	144 ± 6	164 ± 6	130 ± 3	133 ± 5	111 ± 4
Zn (ppm)			62 ± 1	55 ± 6	

Major elements of Fe, Ni, and P were determined by electron microprobe; all other elements were determined by LA-ICP-MS. Errors were calculated as twice the standard error of the mean.

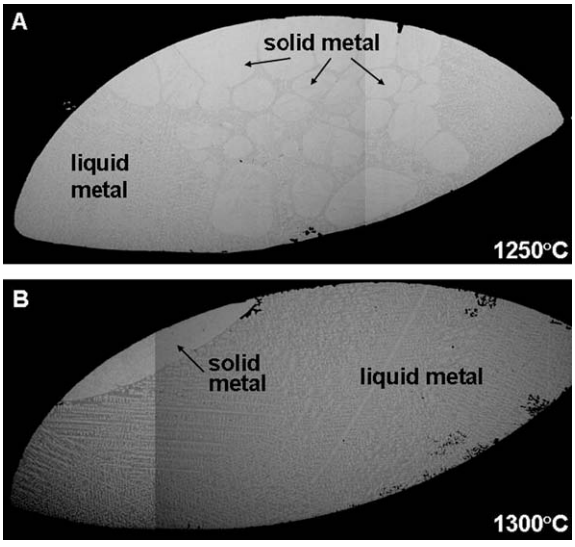

Fig. 1. Back-scattered electron (BSE) images of (A) run #P11, conducted at 1250 °C and (B) run #P4, conducted at 1300 °C, showing the separation of solid metal and liquid metal in the experiments. Solid metal is of a homogeneous composition. A dendritic texture, which formed during quenching of the experiments, can be seen in the liquid metal in both images. The long axis of both experiments is ~5 mm.

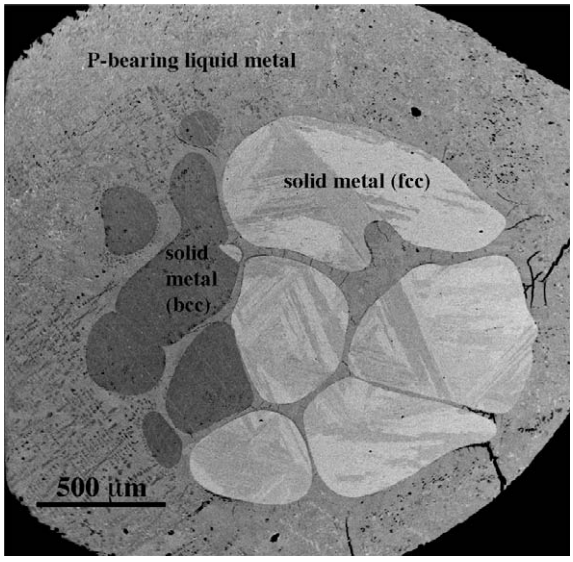

Fig. 2. A back-scattered electron image of run #CC5, with the contrast enhanced to show the three different phases present during the experiment, is shown. All runs contained a P-bearing metallic liquid, which quenched to a dendritic texture, and two solid metal phases, one with an α (bcc) crystal structure and the other with a γ (fcc) crystal structure at the experimental run temperature. For both crystal structures, the solid metal was homogenous; the different scales of gray within the γ-solid metal in this image are due to the crystal orientations of the solid metal and show no compositional differences.

length at 213 nm (UP213, New Wave Research). The laser was operated with a uniform energy density of ~2.6 J/cm^2. Ablation sampling was done in line scan mode using a 30 μm diameter spot and 7 Hz flash rate for the solid metal and 80 μm diameter spot size and 5 Hz flash rate for the liquid metal. The sample was moved at a rate of 10 μm/s during ablation. For each experiment, analysis locations were chosen using backscattered electron and reflected light images. The lengths of the line scans varied depending on the specific features of each run product but were generally 300–1000 μm in length. In general, four or five line scans were conducted in each solid and liquid phase, though where solid metal regions were too small for a line scan, a spot scan was conducted. This analysis approach has proven to be effective for measuring the bulk composition of the quenched metallic liquid in similar previous solid metal/liquid metal experimental samples (Chabot et al., 2003, 2007). Data were collected for the following masses: ^{53}Cr, ^{57}Fe, ^{59}Co, ^{62}Ni, ^{63}Cu, ^{65}Cu, ^{66}Zn, ^{69}Ga, ^{71}Ga, ^{72}Ge, ^{73}Ge, ^{75}As, ^{95}Mo, ^{97}Mo, ^{99}Ru, ^{101}Ru, ^{103}Rh, ^{105}Pd, ^{107}Ag, ^{108}Pd, ^{109}Ag, ^{117}Sn, ^{118}Sn, ^{121}Sb, ^{123}Sb, ^{182}W, ^{183}W, ^{185}Re, ^{188}Os, ^{189}Os, ^{191}Ir, ^{193}Ir, ^{194}Pt, ^{195}Pt, ^{197}Au, ^{206}Pb, ^{208}Pb, and ^{209}Bi. Analyses of solid and liquid metal pairs were accompanied by the average of 3–4 analyses performed on two standard reference materials. These standard materials were SRM NIST 610 for Bi, Pb, and Zn (Pearce et al., 1997) and either NIST 610 or one of the iron meteorites Hoba or Filomena (Walker et al., 2008) for the rest of the elements. These were analyzed before and after the sample analysis, which provided the calibration for determining element concentrations and for constraining instrument drift. Data were processed using the LAMTRACE (Achterberg et al., 2001) software program, which determines element concentrations based on ratios of count rates for samples and standards, known concentrations in the standards, and the known concentration of an internal standard in the unknowns. Analysis by electron microprobe of the major element composition was used to provide Ni as an internal standard for these experiments.

Table 1 provides the compositional measurements for the γ-solid metal/liquid metal runs and Table 2 lists the compositions of the three-phase α−γ-liquid experiments. Errors reported are twice the standard error of the mean. If the measurement for an element was below the detection limit or if the error in a measurement was greater than 25%, then data for that element was not reported in the tables for that phase.

3. RESULTS

3.1. Solid metal/liquid metal partitioning behavior

The solid metal/liquid metal weight ratio partition coefficient for an element E is calculated as:

$$D(\mathrm{E}) = (C_\mathrm{E})^{\text{solid metal}}/(C_\mathrm{E})^{\text{liquid metal}} \quad (1)$$

where C_E is the concentration (in wt%) for the element E in either the solid metal or liquid metal. Partition coefficients determined from the experiments produced in this study are listed in Table 3.

Fig. 3 shows the partitioning results for the major elements of Ni and P plotted as a function of the P-content of the metallic liquid. The partitioning values determined by previous experimental studies (Narayan and Goldstein, 1982; Willis and Goldstein, 1982; Malvin et al., 1986; Jones and Malvin, 1990; all compiled in the Appendix) for D(Ni) and D(P) in the Fe–Ni–P system are also plotted on Fig. 3. There is good agreement between our new experimental results and the results from these four previous studies. Both D(Ni) and D(P) show remarkably constant partitioning values that are independent of the P-content of the metallic liquid, from the P-free system to a value near the Fe–Fe_3P eutectic composition.

The partitioning results for 21 trace elements (not including Zn) in the experiments are plotted against the concentration of P in the metallic liquid in Fig. 4. Our new experimental results are in good agreement with the limited previous experimental determinations of D(Au), D(Ga), D(Ge), and D(Ir) (Narayan and Goldstein, 1982; Willis and Goldstein, 1982; Malvin et al., 1986; Jones and Malvin, 1990; all compiled in the Appendix). D(Ge) and D(Ir) appear slightly higher in our study than the few previous determinations, but the results fall within the combined errors of our work and the previous studies. For the other 17 elements shown in Fig. 4, these data are the first determinations of the γ-solid metal/liquid metal partitioning behavior in the Fe–Ni–P system. Some solid metal/liquid metal partitioning values reported by Jones and Malvin (1990) and Chabot and Drake (2000) involve α-solid metal and liquid metal and are thus not appropriate for comparison to the experimental results of this study. Chabot et al. (2003) report partitioning values for a number of trace elements, but the experiments contain S along with P and thus fall in the more complex Fe–Ni–S–P system.

Many of the trace elements exhibit a slight increase in their solid metal/liquid metal partition coefficients with increasing P-content of the metallic liquid. These elements include As, Au, Ga, Ge, Ir, Os, Pt, Re, and Sb. However, in all cases, the amount of increase in the partition coefficients is fairly minor, with D(Ir) showing the largest increase, amounting to about a factor of six increase from the P-free system to a metallic liquid with nearly 10 wt% P. The less than a factor of two increases in D(Re) and D(Sb) exhibited on Fig. 4 are arguably indistinguishable from constant partitioning behavior.

Some trace elements (Co, Cu, Pd, and Sn) show constant partition coefficients over the entire range of P-contents investigated. Additionally, Ag, Bi, Cr, and Pb have enough scatter and larger error bars in their experimentally determined D values that it is not possible to confidently determine any trend in their partitioning behavior as a function of P-content of the liquid, though it is notable that Ag, Bi, and Pb seem to have systematically lower partition coefficients at higher P concentrations.

Four elements (Mo, Ru, Rh, and W) in our study suggest P-loving tendencies. Like the term chalcophile to

Table 3
Partitioning results for solid metal/liquid metal experiments.

Run #	P24	P20	P22	P25	P11	P4	P1J	P5J	P6J
Temperature (°C)	1100	1125	1150	1200	1250	1300	1350	1400	1450
P (wt%)	8.8 ± 1.1	9.3 ± 1.0	7.9 ± 0.9	7.8 ± 0.9	7.9 ± 1.8	6.0 ± 1.6	4.9 ± 0.8	3.7 ± 1.3	3.1 ± 0.8
D(Ni)	0.88 ± 0.11	0.88 ± 0.12	0.87 ± 0.16	0.87 ± 0.10	0.90 ± 0.03	0.89 ± 0.04	0.90 ± 0.02	0.89 ± 0.03	0.88 ± 0.02
D(P)	0.12 ± 0.07	0.12 ± 0.05	0.13 ± 0.06	0.12 ± 0.06	0.11 ± 0.02	0.11 ± 0.03	0.11 ± 0.02	0.10 ± 0.03	0.11 ± 0.03
D(Ag)	0.11 ± 0.03	0.11 ± 0.02	0.11 ± 0.03	0.11 ± 0.01	0.22 ± 0.04	0.21 ± 0.11			0.18 ± 0.05
D(As)	0.65 ± 0.07	0.68 ± 0.04	0.54 ± 0.05	0.47 ± 0.04	0.57 ± 0.04	0.48 ± 0.04	0.40 ± 0.07	0.37 ± 0.03	0.36 ± 0.02
D(Au)	0.93 ± 0.09	0.96 ± 0.12	0.85 ± 0.12	0.77 ± 0.05	0.87 ± 0.09	0.79 ± 0.04	0.65 ± 0.04	0.55 ± 0.04	0.57 ± 0.03
D(Bi)	0.006 ± 0.002	0.006 ± 0.002	0.006 ± 0.003	0.007 ± 0.002	0.013 ± 0.005				0.013 ± 0.005
D(Co)	1.05 ± 0.04	1.06 ± 0.05	1.03 ± 0.06	1.05 ± 0.05	1.3 ± 0.2	1.3 ± 0.1	1.32 ± 0.09	1.17 ± 0.08	1.28 ± 0.04
D(Cr)				0.68 ± 0.09	1.0 ± 0.1	1.0 ± 0.3	0.87 ± 0.19	1.2 ± 0.2	1.3 ± 0.2
D(Cu)	1.03 ± 0.07	1.01 ± 0.06	0.90 ± 0.04		1.20 ± 0.04	1.16 ± 0.04	1.11 ± 0.07	0.99 ± 0.08	1.00 ± 0.06
D(Ga)	2.6 ± 0.6	2.6 ± 0.6	2.3 ± 0.6	2.0 ± 0.2	2.0 ± 0.2	1.8 ± 0.1	1.3 ± 0.2	1.24 ± 0.20	1.1 ± 0.1
D(Ge)	2.4 ± 0.6	2.4 ± 0.3	2.1 ± 0.4	1.9 ± 0.2	1.9 ± 0.1	1.6 ± 0.1	1.4 ± 0.2	1.10 ± 0.09	1.18 ± 0.07
D(Ir)	9 ± 4	8 ± 2		7 ± 1	6 ± 1	5 ± 1		3.3 ± 0.3	4 ± 1
D(Mo)	0.30 ± 0.03	0.31 ± 0.02	0.34 ± 0.03	0.37 ± 0.03	0.50 ± 0.03	0.58 ± 0.05	0.64 ± 0.07	0.65 ± 0.07	0.69 ± 0.04
D(Os)	9 ± 4	8 ± 2		8 ± 2	7 ± 1	6 ± 1		4 ± 1	5 ± 2
D(Pb)	0.012 ± 0.004	0.012 ± 0.003	0.012 ± 0.005	0.012 ± 0.004	0.03 ± 0.01				0.03 ± 0.01
D(Pd)	0.65 ± 0.05	0.67 ± 0.06	0.59 ± 0.09	0.59 ± 0.07	0.89 ± 0.09	0.65 ± 0.13	0.71 ± 0.04	0.68 ± 0.07	0.69 ± 0.02
D(Pt)	5 ± 2	5 ± 1	4 ± 1	4 ± 1	4 ± 0.4	2.9 ± 0.2	3 ± 1	1.8 ± 0.2	2.1 ± 0.3
D(Re)	5 ± 2	5 ± 1	4 ± 2	4 ± 1	4.7 ± 0.3	4 ± 1		2.8 ± 0.3	3.6 ± 0.8
D(Rh)	1.07 ± 0.06	1.09 ± 0.07	1.08 ± 0.09	1.11 ± 0.07	1.29 ± 0.07	1.33 ± 0.04	1.4 ± 0.2	1.2 ± 0.1	1.4 ± 0.1
D(Ru)	1.3 ± 0.1	1.4 ± 0.1	1.4 ± 0.1	1.4 ± 0.1	1.7 ± 0.1	1.5 ± 0.2	1.9 ± 0.5	1.7 ± 0.1	1.9 ± 0.3
D(Sb)	0.28 ± 0.04	0.31 ± 0.03	0.26 ± 0.05	0.23 ± 0.04	0.32 ± 0.05	0.28 ± 0.06	0.20 ± 0.08	0.21 ± 0.03	0.20 ± 0.03
D(Sn)	0.23 ± 0.03	0.25 ± 0.03	0.21 ± 0.05	0.19 ± 0.04	0.27 ± 0.03	0.26 ± 0.04	0.19 ± 0.05	0.19 ± 0.03	0.18 ± 0.03
D(W)	0.96 ± 0.09	1.00 ± 0.09	0.99 ± 0.09	1.05 ± 0.09	1.32 ± 0.09	1.41 ± 0.04	1.5 ± 0.4	1.2 ± 0.1	1.4 ± 0.2

Errors are $\pm 2\sigma$. *D*(Ni) and *D*(P) were calculated using electron microprobe data. All other partition coefficients were calculated using LA-ICP-MS data.

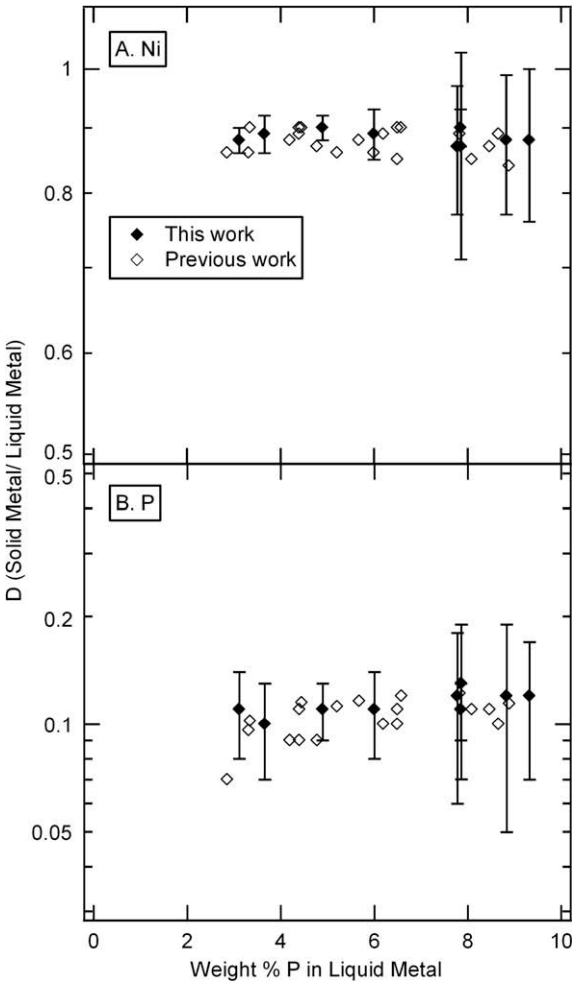

Fig. 3. The solid metal/liquid metal partition coefficients (D) for values for (A) Ni and (B) P are plotted as a function of the P concentration of the metallic liquid (in wt%). The partition coefficients for P remain constant despite an increase in P concentration. These results are in agreement with the limited previous experiments (Narayan and Goldstein, 1982; Willis and Goldstein, 1982; Malvin et al., 1986; Jones and Malvin, 1990). Error bars are $\pm 2\sigma$.

describe S-loving behavior and the term anthracophile to describe C-loving behavior (Chabot et al., 2006), we adopt the term phosphorophile to describe P-loving behavior. As shown in Fig. 4, Mo is the best example of phosphorophile behavior, showing a decrease of slightly more than a factor of two in its partition coefficient with increasing P-content of the metallic liquid. The three elements of Rh, Ru, and W may suggest a slight decrease in their partition coefficients with increasing P-content of the metallic liquid, but the decrease is less than a factor of two and their D values are also generally consistent with essentially constant partitioning behavior. Though these four elements may exhibit phosphorophile tendencies, the overall effect of P on their solid metal/liquid metal partitioning behavior is minor.

3.2. Solid metal/liquid metal parameterization method

Models offer some explanation for the observed solid metal/liquid metal partitioning behavior of elements. Jones and Malvin (1990) suggested that metallic liquid could be envisioned as being composed of two types of "domains:" non-metal-free domains and non-metal-bearing domains. In their model, in which a metallic liquid in the Fe–S system is composed of Fe domains and FeS domains, Jones and Malvin (1990) had success at matching the functional form of the trends of partition coefficients for siderophile elements in the Fe–S system, where some partitioning values increase significantly with increasing S-content of the metallic liquid. Chabot and Jones (2003) revised the method by which the domains in the metallic liquid were calculated but kept the same fundamental concept for the model as Jones and Malvin (1990), that the metallic liquid was composed of domains and the availability of those domains controlled the partitioning behavior. In both models, in the Fe–S system, siderophile elements have strongly increasing solid metal/liquid metal partition coefficients with increasing S-content of the metallic liquid because siderophile elements strongly prefer the Fe domains to the FeS domains and as the S-content of the metallic liquid increases, the fraction of Fe domains decreases.

Chabot and Jones (2003) expressed this dependency of the partition coefficients of siderophile elements on the Fe domains as:

$$\frac{1}{D} = \frac{(Fe\ domains)^{\beta}}{D_0} \tag{2}$$

where D is the solid metal/liquid metal partition coefficient, D_o is the partition coefficient in the non-metal-free system, and β is a constant specific to the element being modeled. β and D_o are both determined through fits to the data. The quantity of *Fe domains* is the fraction of non-metal-free domains in the metallic liquid and the calculation of this quantity depends on the speciation of the non-metal in the metallic liquid. For the Fe–Ni–S–P system, assuming speciations of FeS and Fe_3P, *Fe domains* is calculated as:

$$Fe\ domains = \frac{(1 - 2X_S - 4X_P)}{(1 - X_S - 3X_P)} \tag{3}$$

By combining Eqs. (2) and (3), it can be seen that the model of Chabot and Jones (2003) predicts that each element can be fit in the Fe–Ni–S–P system with a single value of D_o and a single value of β. Having a single value per element for D_o would be expected, as D_o represents the partition coefficient in the S-free, P-free system. In contrast, for β, Jones and Malvin (1990) used different values for a given element when modeling the element in the Fe–Ni–S and Fe–Ni–P systems. However, with their revised method of calculating the *Fe domains*, Chabot and Jones (2003) had success at modeling experimental data for both D(Ge) and D(Ir) from the Fe–Ni–S, Fe–Ni–P, and Fe–Ni–S–P systems using a single β value for each element.

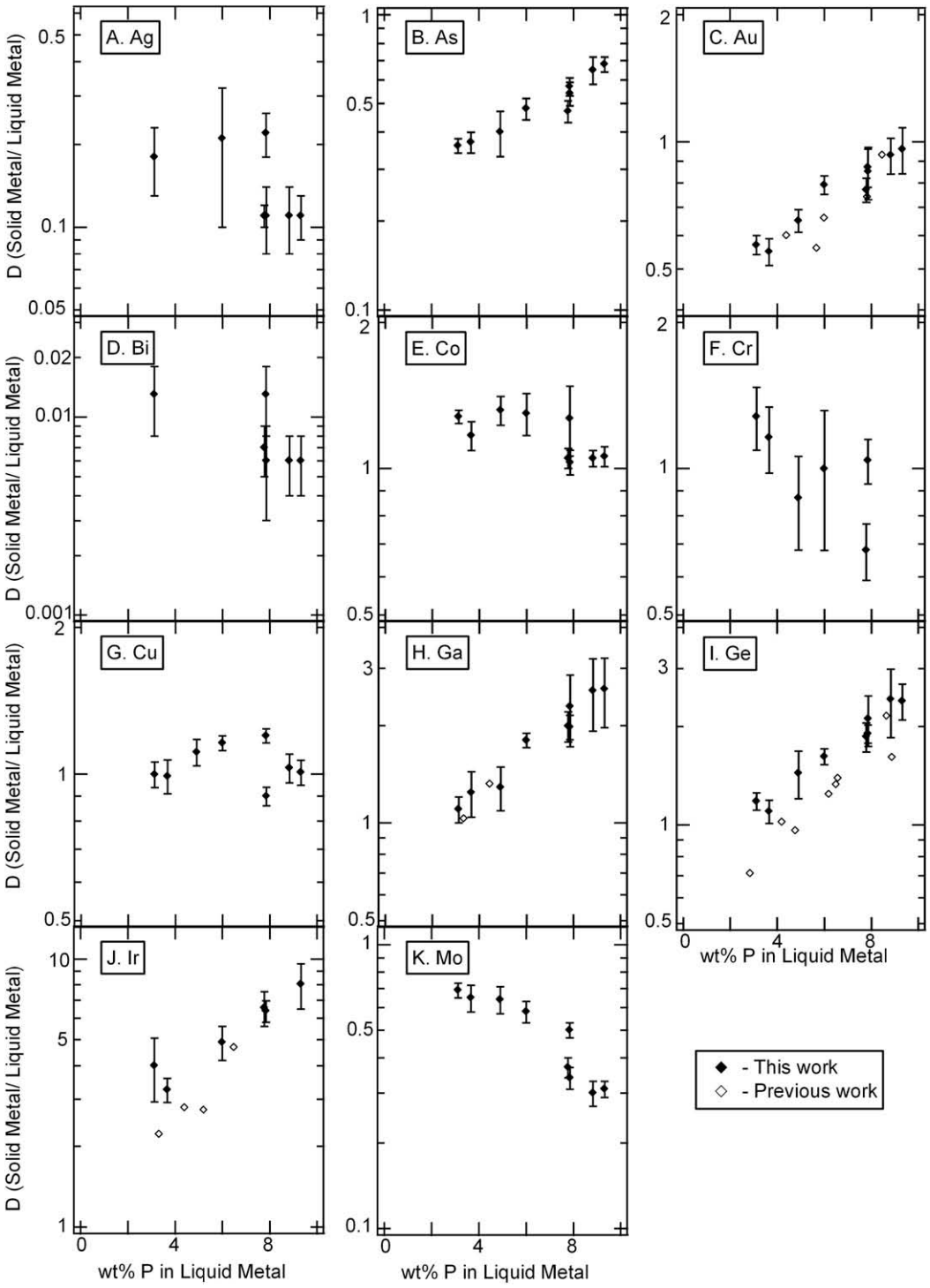

Fig. 4. The solid metal/liquid metal partition coefficients (D) for values for (A) Ag, (B) As, (C) Au, (D) Bi, (E) Co, (F) Cr, (G) Cu, (H) Ga, (I) Ge, (J) Ir, (K) Mo, (L) Os, (M) Pb, (N) Pd, (O) Pt, (P) Re, (Q) Rh, (R) Ru, (S) Sb, (T) Sn, and (U) W are plotted as a function of the P concentration of the metallic liquid (in wt%). These results are in agreement with the limited previous experiments (Narayan and Goldstein, 1982; Willis and Goldstein, 1982; Malvin et al., 1986; Jones and Malvin, 1990). Error bars are $\pm 2\sigma$.

As mentioned and detailed in the Appendix, previous experimental data for solid metal/liquid metal partitioning in the Fe–Ni–P system are limited. Data presented in this study greatly increase the available partitioning data in the Fe–Ni–P system. Thus, these new data can be used to more thoroughly test the parameterization model of Chabot and Jones (2003). The parameterization model of Chabot and Jones (2003) predict that these new experimental

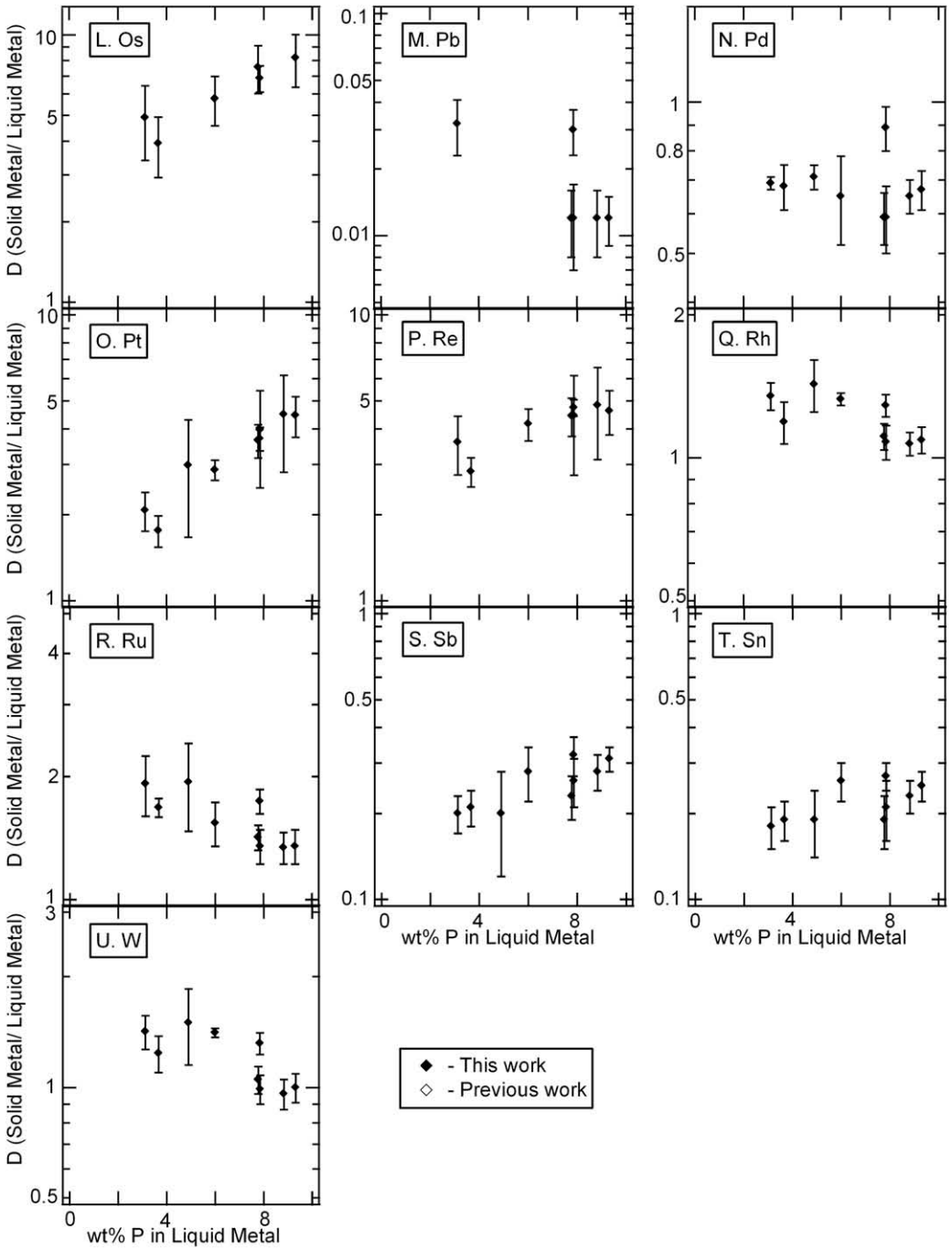

Fig. 4 (*continued*)

data will fall on their fitted equation for each element, even though that fit was determined essentially from data in the Fe–Ni–S system and our new data are from the Fe–Ni–P system.

3.3. Parameterization of new solid metal/liquid metal results

Fig. 5 shows the partition coefficients for 12 elements parameterized by Chabot and Jones (2003) plotted against the *Fe domains*, as calculated using Eq. (3). D(Ge), D(Ir), and D(Os) are all generally well fit by the parameterized expression given in Chabot and Jones (2003). This suggests that for these three elements, this parameterization can be used for the Fe–Ni–S, Fe–Ni–P, or mixed Fe–Ni–S–P system. Table 4 lists the values of β and D_o for these parameterizations.

The parameterizations of Chabot and Jones (2003) are only appropriate to apply to elements that show increas-

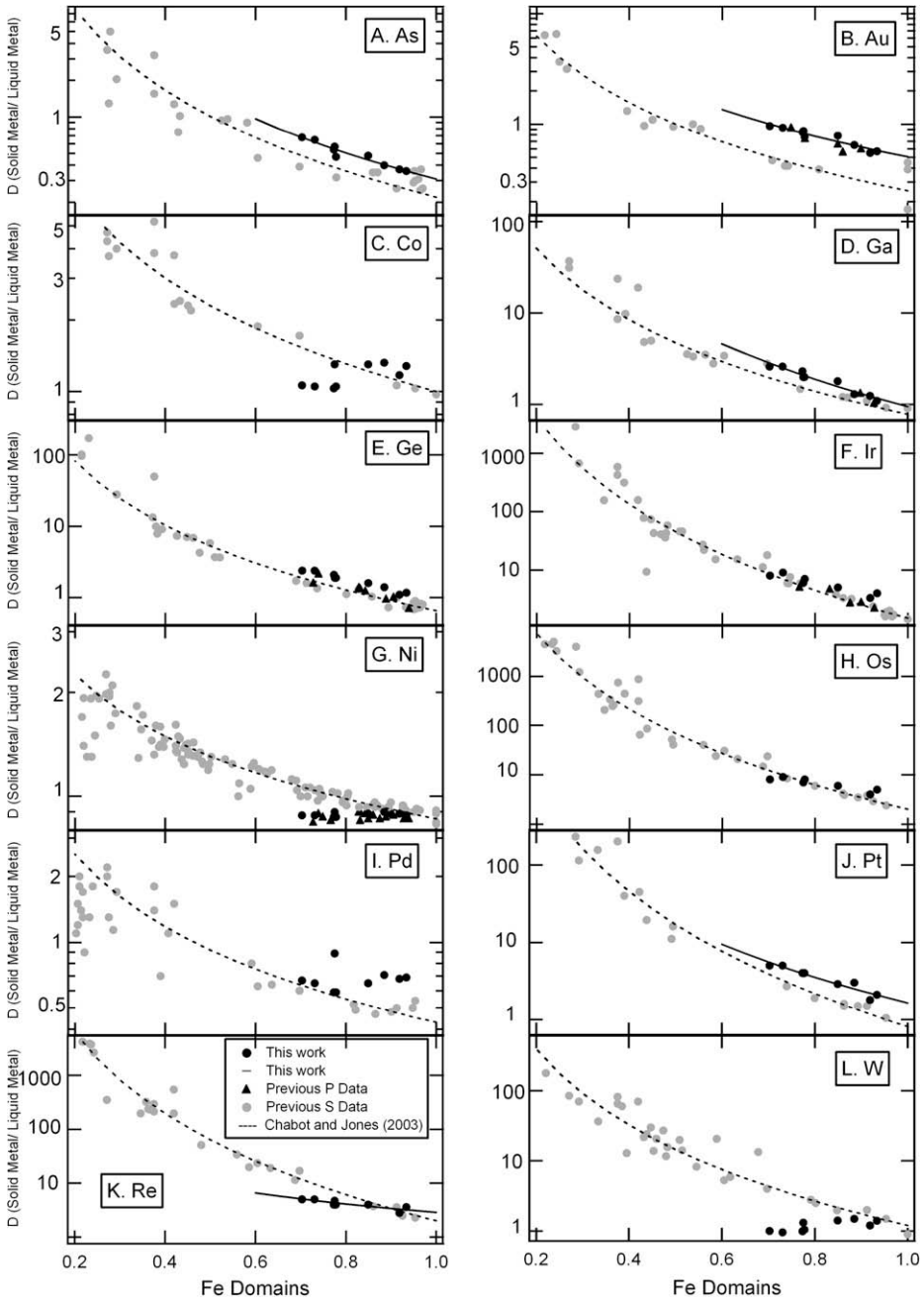

Fig. 5. Our results for partitioning in the Fe–Ni–P system are compared to the predicted parameterizations of Chabot and Jones (2003) for the elements (A) As, (B) Au, (C) Co, (D) Ga, (E) Ge, (F) Ir, (G) Ni, (H) Os, (I) Pd, (J) Pt, (K) Re, and (L) W.

ing partition coefficients with increasing non-metal content of the metallic liquid, as such elements are behaving as siderophile elements in the system and are attracted only to the non-metal-free domains. If an element exhibits a constant partitioning value that is independent of the metallic liquid composition, then it would suggest that the element is equally accepting of both types of domains in the metallic liquid, and this preference is not expressed appropriately in Eq. (2). Similarly, if an element has a decreasing partitioning value with increasing non-metal content, then that element is attracted to the non-metal-bearing domains and should be expressed as such and not as a function of the *Fe domains* in Eq. (2). Thus, it is expected that the partitioning behaviors of Co, Ni, Pd, and W in the Fe–Ni–P system would not fall on the parameterized expression for their behaviors in the Fe–Ni–S system. Indeed, this is what is seen in Fig. 5. In the Fe–Ni–S system, Co, Ni, Pd, and W behave as siderophile elements and have increasing partition coefficients with increasing S-content of the metallic li-

Table 4
Values for fitted parameterizations.

For use in:	D_o (wt%)	β
Fe–Ni–P system only		
As	0.31	2.2
Au	0.51	1.9
Ga	0.95	3.1
Pt	1.6	3.4
Re	2.9	1.6
Fe–Ni–P–S system		
Ge	0.66[a]	3.0[a]
Ir	1.5[a]	4.9[a]
Os	2.0[a]	5.1[a]

[a] Values from the parameterizations of Chabot and Jones (2003). All others from this work.

quid, while in the Fe–Ni–P system, these elements have constant partitioning values or even a slightly decreasing value in the case of D(W).

However, for the elements of As, Au, Ga, Pt, and Re, the parameterized expressions of Chabot and Jones (2003) would be predicted to match the partitioning values in the Fe–Ni–P system. As shown in Fig. 5, the expressions of Chabot and Jones (2003) fail to match the new P-bearing experimental data. The behavior of D(Re) in the Fe–Ni–P system is nearly constant and thus may potentially be excused from failing to be fit. However, As, Au, Ga, and Pt clearly show increases in their partition coefficients with decreasing *Fe domains* in the metallic liquid but fall on different trends than the S-bearing data. The model of Chabot and Jones (2003) thus fails to account for the behavior of these elements with a single β and D_o value.

It is possible that the speciation of P may be something other than Fe_3P (i.e., Fe_2P and Fe_5P_2). However, since all elements need to be fit with the same Fe domains calculation (since the domains describe the metallic liquid and all of the trace elements are together in that liquid), changing the speciation only serves to change which elements are fit. If all elements were offset to higher values, the Fe domains could be the issue, but changing the Fe domains calculation would result in D(Ge), D(Ir), and D(Os) no longer being fit well by the parameterized equations.

Additionally, much of the discrepancy between the data in the Fe–Ni–P and Fe–Ni–S systems shown on Fig. 5 arise from the partitioning value suggested in the P-free, S-free system, when Fe domains has a value of one. In the P-free system, the choice of the speciation of P in the liquid has no effect on the calculated Fe domains, because all of the liquid is Fe domains. A troubling observation of Fig. 5 is the suggestion of different D_o values in the Fe–Ni–S and Fe–Ni–P systems. This discrepancy is most pronounced in Fig. 5 for Au. We note that our Au data are in good agreement with previous P-bearing D(Au) values (even those calculated from elemental concentrations measured using electron microprobe as opposed to LA-ICP-MS), suggesting the offset seen in Fig. 5 is not an artifact of our analytical or experimental methods; the limited previous experimental D(Au) data in the Fe–Ni–P system suggested a different D_o value than Au-bearing experiments conducted in the Fe–Ni–S system, even prior to the data we present here. It is expected that in the S-free, P-free system, when the metallic liquid is composed of only *Fe domains*, an element would have a unique solid metal/liquid metal partitioning value.

We currently do not have an explanation as to why different values for D_o are suggested by data from the Fe–Ni–S and Fe–Ni–P systems for some elements (particularly Au) or as to why some elements (Ge, Ir, and Os) are well fit by the Fe–Ni–S–P parameterization in systems containing only P as a light element, while others are not. One hypothesis is that the higher P concentrations in the solid metal in the Fe–Ni–P system as compared to the essentially zero S concentration in the solid metal in the Fe–Ni–S system is an important difference which is influencing the partitioning behavior. There is some support for this hypothesis, in that partitioning in the Fe–Ni–C system, which also has high levels of C in the solid metal, suggests a similar discrepancy between suggested D_o values in the Fe–Ni–S and Fe–Ni–C systems for some elements (Chabot et al., 2006). Solid metal/liquid metal experiments in the light element free Fe–Ni system are planned but will likely require a different experimental set-up than evacuated silica tubes used in this study. Also, limited experiments have been conducted in the Fe–Ni–S–P system (compiled in Chabot and Jones, 2003), and additional partitioning data from this multi-light-element system would provide further insight into the effects of S and P solid metal/liquid metal partition coefficients. This is an important discrepancy that needs to be resolved, especially as it involves understanding the partitioning behavior of Au. Gold has become the preferred element to use when plotting iron meteorite trends and modeling the crystallization of iron meteorite groups (e.g. Wasson, 1999; Wasson and Richardson, 2001; Chabot, 2004). Thus, any uncertainty in the partitioning behavior of Au, and the D_o value for Au, will affect the ability to use this element to interpret the history and evolution of iron meteorites.

As a current approach, for elements that exhibit different partitioning behaviors in the Fe–Ni–S and Fe–Ni–P system, a method like that used in Jones and Malvin (1990) is needed for these elements. Jones and Malvin (1990) used separate β values for the Fe–Ni–P and Fe–Ni–S systems and treated partitioning in the combined Fe–Ni–S–P system as a weighted average of the partitioning behaviors from the two end-member systems, assuming linear behavior. Jones and Malvin (1990) also calculated D_o values by using a weighted average of the D_o values from the Fe–Ni–S and Fe–Ni–P system. Table 4 provides β and D_o values determined by using Eqs. (2) and (3) but fitting only data from the Fe–Ni–P system for the five elements of As, Au, Ga, Pt, and Re.

3.4. Partitioning between α and γ-solid metal

In total, five three-phase α−γ-liquid experiments were conducted, with slight variations in temperature

Table 5
Partitioning values from three-phase α-solid metal, γ-solid metal, and liquid metal.

Element	$D(\alpha/\gamma)$[a]	$D(\gamma/\text{liq. met.})$[a]
Ag	1.02 ± 0.08	0.13 ± 0.01
As	1.03 ± 0.04	0.59 ± 0.02
Au	0.85 ± 0.05	0.85 ± 0.05
Bi	1.56 ± 0.15	0.009 ± 0.001
Co	0.98 ± 0.03	1.1 ± 0.03
Cr	1.11 ± 0.13	0.62 ± 0.05
Cu	0.86 ± 0.04	0.99 ± 0.04
Fe	1.004 ± 0.004	1.11 ± 0.01
Ga	0.92 ± 0.03	2.5 ± 0.1
Ge	0.88 ± 0.04	2.2 ± 0.1
Ir	0.60 ± 0.02	7.4 ± 0.5
Mo	1.38 ± 0.06	0.33 ± 0.01
Ni	0.83 ± 0.01	1.18 ± 0.02
Os	0.70 ± 0.03	7.9 ± 0.6
P	1.93 ± 0.09	0.13 ± 0.01
Pb	1.55 ± 0.12	0.018 ± 0.003
Pd	0.84 ± 0.05	0.57 ± 0.02
Pt	0.62 ± 0.02	4.0 ± 0.2
Re	0.94 ± 0.05	5.0 ± 0.2
Rh	0.82 ± 0.05	1.02 ± 0.04
Ru	0.85 ± 0.04	1.34 ± 0.04
Sb	1.09 ± 0.05	0.24 ± 0.01
Sn	1.39 ± 0.06	0.23 ± 0.01
W	1.33 ± 0.04	1.10 ± 0.03
Zn	1.01 ± 0.14	1.0 ± 0.1

[a] D values were calculated as the weighted average of the five runs detailed in Table 2. The error is twice the weighted error. The weighted average wt% P in the liquid metal for the five runs was 8.7 ± 0.3.

(1100–1150 °C) and starting bulk compositions. All five experiments produced similar α/γ (bcc/fcc) partitioning behaviors that were indistinguishable within error. Thus, the results presented are weighted averages from these five runs. Table 5 gives the α/γ partition coefficients and the γ-solid metal/liquid metal partition coefficients. The γ-solid metal/liquid metal partition coefficients are in excellent agreement with the trends and values in Table 3.

As listed in Table 5 and shown graphically in Fig. 6, all of the elements measured have α/γ partitioning values between 0.60 and 1.93. In the experiments, the α/γ partitioning ratios for the major elements of Fe (1.004), Ni (0.83), and P (1.93) are consistent with the Fe–Ni–P phase diagram (Doan and Goldstein, 1970). In general, the fact that all of the trace elements in Table 5 have α/γ partitioning ratios so close to unity indicates that Fe alloy crystal structure has only a minor influence on the partitioning behaviors of all of the 22 trace elements studied. For the diverse set of 22 trace elements examined by this work, there is a factor of three of absolute fractionation among them due to effects from the solid Fe alloy crystal structure, though it could also possibly be due to high temperature. Existing data (Watson et al., 2008) show that low-temperature equilibration leads to large differences in D-value.

As shown in Fig. 6, a few elements do exhibit more than a 20% difference for partitioning between α and γ Fe alloy solids, and some similarities between the natural crystal structure of an element and its preference for α versus γ solids are observed. For example, of all the trace elements in Table 2, Cr, W, and Mo are the only three with a bcc structure and all three of these elements show a preference for the α-solid phase as compared to the γ-solid metal. In contrast, the highly siderophile elements of Ir and Pt, both fcc elements, show a slight preference for the γ-solid over the α-solid. However, Os, which is an hcp (hexagonal close-packed) element, shows a preference for the γ-solid while the neighboring element of Re, which is also hcp, has a α/γ partitioning ratio of just 0.94, very close to unity. Additionally, Pb, a fcc element,

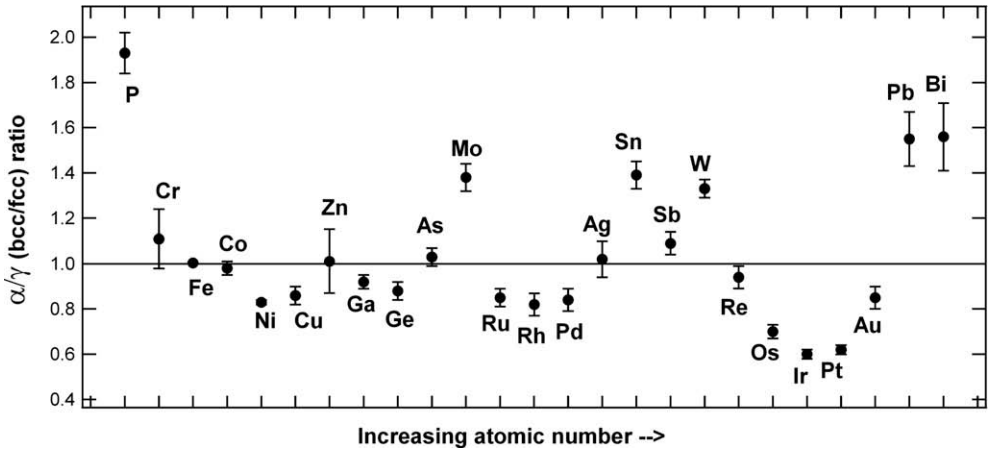

Fig. 6. The α/γ concentration ratios determined by our experiments are plotted in order of increasing atomic number. A ratio of one, shown as a solid line, indicates that an element has no preference for the α structure relative to the γ structure. All 22 elements present at trace levels have α/γ ratios close to unity, suggesting that an α versus γ Fe alloy crustal structure has only a minor affect on the partitioning behaviors of these elements.

shows the second largest preference for the α-solid over the γ-solid of all of the elements in Table 5. Thus, a simple relationship between an element's natural crystal structure and its α/γ partitioning ratio is not observed.

In a study of the distribution of platinum group elements and Re between phases in iron meteorites, Hirata and Nesbitt (1997) noted a correlation between ionic size and the partitioning ratios of these elements between kamacite (α) and Ni-rich phases including taenite (γ); they suggested that ionic radius was the controlling mechanism, resulting in a smooth progression with the order being (from small to large) Ir–Os–Pt–Re–Rh–Ru–Pd. Given that bonding in these compounds is metallic, several difficulties arise in assigning accurate "ionic" radii to them. The α/γ partitioning results given in Table 5 and Fig. 6 do not show any such progression for these same elements. A laser ablation ICP-MS study by Mullane et al. (2004) concluded that the kamacite/taenite distribution of HSE in pallasites and iron meteorites was controlled by the atomic size of the elements. Our experimental dataset, which includes many elements in addition to HSE, does not show a simple relationship between α/γ partitioning and an element's atomic size.

4. IMPLICATIONS FOR IRON METEORITES

The main motivation for this project was to determine the effect of P on the distribution of trace elements during the evolution of iron meteorites. Our experimental results have applications to understanding both the crystallization of iron meteorites and the subsolidus formation of the Widmanstätten pattern.

During the crystallization of iron meteorites, the nonmetal content of the metallic liquid will have an effect on the distribution of trace elements between the forming solid metal and the residual liquid metal. However, our results indicate that for the 22 elements examined experimentally, the effect of P on solid metal/liquid metal partitioning behavior is relatively minor. For the majority of these elements, the partition coefficients changed only by about a factor of two or less, even though the P-content of the metallic liquid varied from about 3 wt% to over 9 wt%, close to the Fe–Fe_3P eutectic composition of 10 wt% P (Gustafson, 1990). Even D(Ir), which exhibited the largest change in its partition coefficient, varied by only about a factor of six. This is in marked contrast to the effect of S on the partitioning behavior of many of these elements. As seen on Fig. 5, D(Ir) varies from the S-free system to a S-content near the Fe–FeS eutectic of 31 wt% D(Ir) increases by nearly three orders of magnitude. Other elements such as Re and Os show equally large increases in their D values with increasing S in the metallic liquid. For all of the elements shown on Fig. 5, the influence of S is considerably larger than the influence of P on the solid metal/liquid metal partitioning value when examined over the large range of S contents versus the more limited range of P concentrations.

Thus, if an iron meteorite is crystallizing from a single metallic liquid that contains both S and P, the effect of P on the distribution of elements between the crystallizing solid and residual liquid will be minor in comparison to the effect of S, given the larger concentrations of S relative to P believed to be involved during the crystallization of most iron meteorites. Our results suggest that fractional crystallization models involving Fe–Ni–S–P liquids that do not include effects from P on elemental partition coefficients (Chabot, 2004) will still result in first order crystallization trends appropriate for interpreting the evolution of iron meteorites if the effects of S on partitioning behavior are appropriately included in the modeling effort.

However, as fractional crystallization proceeds, a Fe–Ni–S–P liquid will become enriched in both S and P. A large liquid immiscibility field exists in the Fe–S–P system (Raghavan, 1988). It has been suggested that some iron meteorite groups (i.e., IIAB and IIIAB) very likely encountered liquid immiscibility in the Fe–Ni–S–P system during their crystallization histories (Ulff-Møller, 1998; Chabot and Drake, 2000). If liquid immiscibility were encountered, two metallic liquids would form, with one liquid being S-rich and the other being P-rich. Knowledge of the effects of both S and P on the partitioning behaviors of elements would thus be needed to interpret and model the distribution of elements between these two immiscible liquids. Modeling studies of Ulff-Møller (1998) and Chabot and Drake (1999) have shown how effects from both S and P can be incorporated into models of iron meteorite crystallization. However, prior to our new experimental work presented here, the effect of P on the behavior of trace elements was not well constrained. Using our new data, these late stage processes can be modeled for the first time for many trace elements by future studies.

The Fe–Ni phases of kamacite (α) and taenite (γ) are found in iron meteorites, making up the widely recognized Widmanstätten pattern in some cases. The Widmanstätten pattern forms as a subsolidus reaction in iron meteorites and is used to deduce the cooling rates of iron meteorites (e.g. Yang and Goldstein, 2005). Measured iron meteorite kamacite/taenite partitioning values have been reported to vary from <0.1 to >3, resulting in over an order of magnitude fractionations among siderophile elements (Rasmussen et al., 1988; Hirata and Nesbitt, 1997; Campbell and Humayun, 1999; McDonough et al., 1999; Hsu et al., 2000; Mullane et al., 2004). However, significant discrepancies exist among the kamacite/taenite partition coefficients reported by these different studies. For some elements, such as Ir, kamacite/taenite partition coefficients both >1 and <1 have been reported. Other studies have demonstrated that kamacite/taenite partition coefficients can be strongly affected by the position within the taenite grain that is measured (e.g. Goldstein, 1967; Watson et al., 2005; Ash et al., 2007). Thus, determining kamacite/taenite values for iron meteorites requires additional work to reach a consensus as to appropriate values.

Once well-determined kamacite/taenite partitioning values are available from iron meteorites, the results can be compared to our experimentally determined α/γ partition coefficients. Our α/γ partition coefficients are from experiments conducted at higher temperatures than the subsolidus formation of kamacite/taenite in iron meteorites, and will likely be found to differ from the latter. These differences could be the result of temperature variation. At temperatures pertinent to Widmanstätten formation, α/γ partition coefficients tend to increase in magnitude with cooling. In other words, the equilibrium concentrations of trace elements in each phase appear to diverge (which is, in part, what is responsible for the development of the characteristic M-shaped profiles observed in iron meteorites (Campbell and Humayun, 1999; Watson et al., 2005)). At temperatures of ~400 °C, estimates of equilibrium partition coefficients of various siderophile elements vary by close to an order of magnitude (Watson et al., 2008). This strong effect of temperature may continue at even higher temperatures, resulting in the relatively smaller variation of partition coefficients observed here. A complete temperature study has not been undertaken here due to the very small three-phase field. Furthermore, differences could result from the effects of variations in P concentration. If this is the case, the differences in partition coefficients between our P-bearing α/γ experiments and kamacite–taenite in iron meteorites may be the low-temperature equivalent of partitioning differences resulting from varying P concentration in our higher-temperature solid metal–liquid metal experiments. Finally, it is assumed that these experiments have reached equilibrium. Equilibrium was not achieved between the kamacite and taenite in iron meteorites, where M-shaped concentration gradients of Ni (Wasson, 1985, p. 89) and many siderophile elements are typically preserved in taenite.

ACKNOWLEDGMENTS

We would like to thank John Jones (JSC) for discussion on experimental technique, Tim Gooding (NMNH) and Vern Lauer (JSC) for their assistance/instruction with vacuum sealing silica tubes, and Lisa Collins for weighing out and mixing powders. In addition, we would like to thank Jijin Yang, David Mittlefehldt and two anonymous reviewers for their comments and suggestions for improvements to this paper. This work was funded by NASA Grants NNG06GF56G to T.J. McCoy, NNG06GI13G to N.L. Chabot, NNG04GG17G to W.F. McDonough, and NSF EAR0337621 grant to W.F. McDonough.

APPENDIX A. PREVIOUS Fe–Ni–P SOLID METAL/LIQUID METAL EXPERIMENTS

Table A1 details previous partitioning values determined in the Fe–Ni–P by experiments that involved (γ)-solid metal and liquid metal. Some solid metal/liquid metal partitioning values reported by Jones and Malvin (1990) and Chabot and Drake (2000) are between α-solid metal and liquid metal and are thus not appropriate for comparison to our experimental results. Chabot et al. (2003) report partitioning values for a number of trace elements, but their exper-

Table A1
Results from previous partitioning studies in the Fe–Ni–P system.

Reference	Run #	wt% P (liq.)	*D*(Au)	*D*(Ga)	*D*(Ge)	*D*(Ir)	*D*(Ni)	*D*(P)
Narayan and Goldstein (1982)	E11	8.89 ± 0.41			1.61 ± 0.14		0.84 ± 0.03	0.114 ± 0.005
Narayan and Goldstein (1982)	E5	6.58 ± 0.52			1.39 ± 0.07		0.90 ± 0.01	0.12 ± 0.01
Narayan and Goldstein (1982)	E4	6.20 ± 0.16			1.24 ± 0.07		0.89 ± 0.02	0.10 ± 0.003
Narayan and Goldstein (1982)	E10	4.78 ± 0.48			0.96 ± 0.06		0.87 ± 0.02	0.09 ± 0.01
Narayan and Goldstein (1982)	E8	2.86 ± 0.40			0.71 ± 0.02		0.86 ± 0.02	0.07 ± 0.01
Willis and Goldstein (1982)	12a	3.35 ± 0.16		1.03 ± 0.04			0.90 ± 0.01	0.102 ± 0.006
Willis and Goldstein (1982)	12b	4.45 ± 0.33		1.32 ± 0.05			0.90 ± 0.02	0.115 ± 0.009
Willis and Goldstein (1982)	13a	5.68 ± 0.28	0.56 ± 0.05				0.88 ± 0.03	0.116±0.007
Willis and Goldstein (1982)	13b	7.83 ± 0.31	0.74 ± 0.08				0.89 ± 0.01	0.122 ± 0.005
Willis and Goldstein (1982)	14	5.21 ± 0.33				2.73 ± 0.36	0.86 ± 0.02	0.112 ± 0.008
Willis and Goldstein (1982)	15	3.32 ± 0.27				2.22 ± 0.19	0.86 ± 0.02	0.096 ± 0.004
Malvin et al. (1986)	23C	6.5				4.67	0.90	0.10
Malvin et al. (1986)	23E	6.5			1.33		0.85	0.11
Malvin et al. (1986)	23G	6.0	0.66				0.86	0.11
Malvin et al. (1986)	23B	4.4				2.79	0.89	0.09
Malvin et al. (1986)	23D	4.2			1.02		0.88	0.09
Malvin et al. (1986)	23F	4.4	0.6				0.90	0.11
Jones and Malvin (1990)	24	8.09				5.07	0.85	0.11
Jones and Malvin (1990)	25	8.66			2.15		0.89	0.10
Jones and Malvin (1990)	26	8.47	0.93				0.87	0.11

Errors given as ±1σ.

iments contain S along with P and thus fall in the more complex Fe–Ni–S–P system.

REFERENCES

Achterberg E. V., Ryan C. G., Jackson S. E. and Griffin W. L. (2001) Appendix 3: Data reduction software for LA-ICP-MS. In *Laser Ablation-ICP-MS in the earth sciences* (ed. P. Sylvester), vol. 29. Mineralogical Association of Canada, Short Course Series, 243 pp.

Ash R. D., Luong M. V., Walker R. J., McDonough W. F. and McCoy T. J. (2007) Trace element fractionation in kamacite and taenite in IVA irons. *Lunar Planet. Sci. XXXVIII*. Lunar and Planetary Institute, Houston (CD-ROM). #2383 (abstr.).

Buchwald V. F. (1975). *Handbook of Iron Meteorites*, vol. 1. University of California Press, Berkeley.

Campbell A. J. and Humayun M. (1999) Trace element microanalysis in iron meteorites by laser ablation ICPMS. *Anal. Chem.* **71**, 939–946.

Chabot N. L. (2004) Sulfur contents of the parental metallic cores of magmatic iron meteorites. *Geochim. Cosmochim. Acta* **68**, 3607–3618.

Chabot N. L. and Drake M. J. (1997) An experimental study of silver and palladium partitioning between solid and liquid metal, with applications to iron meteorites. *Meteorit. Planet. Sci.* **32**, 637–645.

Chabot N. L. and Drake M. J. (1999) Crystallization of magmatic iron meteorites: the role of mixing in the molten core. *Meteorit. Planet. Sci.* **34**, 235–246.

Chabot N. L. and Drake M. J. (2000) Crystallization of magmatic iron meteorites: the effects of phosphorous and liquid immiscibility. *Meteorit. Planet. Sci.* **35**, 807–816.

Chabot N. L. and Jones J. H. (2003) The parameterization of solid metal–liquid metal partitioning of siderophile elements. *Meteorit. Planet. Sci.* **38**, 1425–1436.

Chabot N. L., Campbell A. J., Jones J. H., Humayun M. and Agee C. B. (2003) An experimental test of Henry's Law in solid metal–liquid metal systems with implications for iron meteorites. *Meteorit. Planet. Sci.* **38**, 181–196.

Chabot N. L., Campbell A. J., Jones J. H., Humayun M. and Lauer, Jr., H. V. (2006) The influence of carbon on trace element partitioning behavior. *Geochim. Cosmochim. Acta* **70**, 1322–1335.

Chabot N. L., Saslow S. A., McDonough W. F. and McCoy T. J. (2007) The effect of Ni on element partitioning during iron meteorite crystallization. *Meteorit. Planet. Sci.* **42**, 1735–1750.

Doan, Jr., A. S. and Goldstein J. I. (1970) The ternary phase diagram, Fe–Ni–P. *Metall. Trans.* **1**, 1759–1767.

Goldstein J. I. (1967) Distribution of Germanium in the metallic phases of some iron meteorites. *J. Geophys. Res.* **72**, 4689–4696.

Gustafson P. (1990) *Report IM-2566*. Institute of Metals Research, Stockholm, p. 2549.

Haack H. and McCoy T. J. (2003) Iron and stony-iron meteorites. In *Meteorites, comets, and planets* (ed. A. M. Davis). *Treatise on Geochemistry* (eds. H. D. Holland and K. K. Turekian), vol. 1. Elsevier-Pergamon, Oxford. pp. 325–346.

Hirata T. and Nesbitt R. W. (1997) Distribution of platinum group elements and rhenium between metallic phases of iron meteorites. *Earth Planet. Sci. Lett.* **147**, 11–24.

Hsu W., Huss G. R. and Wasserburg G. J. (2000) Ion probe measurements of Os, Ir, Pt, and Au in individual phases of iron meteorites. *Geochim. Cosmochim. Acta* **64**, 1133–1147.

Jones J. H. and Drake M. J. (1983) Experimental investigations of trace element fractionation in iron meteorites, II: the influence of sulfur. *Geochim. Cosmochim. Acta* **47**, 1199–1209.

Jones J. H. and Malvin D. J. (1990) A nonmetal interaction model for the segregation of trace metals during solidification of Fe–Ni–S, Fe–Ni–P, and Fe–Ni–S–P alloys. *Metall. Trans. B* **21B**, 697–706.

Malvin D. J., Jones J. H. and Drake M. J. (1986) Experimental investigations of trace element fractionation in iron meteorites. III: Elemental partitioning in the system Fe–Ni–S–P. *Geochim. Cosmochim. Acta* **50**, 1221–1231.

McDonough W. F., Horn I., Lange D. and Rudnick R. L. (1999) Distribution of platinum group elements between phases in iron meteorites. *Lunar and Planet. Sci. XXX*. Lunar and Planetary Institute, Houston (CD-ROM). #2062 (abstr.).

Mullane E., Alard O., Gounelle M. and Russell S. S. (2004) LA-ICP-MS study of IAB and IIIAB irons and pallasites: sub-solidus HSE behaviour. *Meteorit. Planet. Sci.* **39**.

Narayan C. and Goldstein J. I. (1982) A dendritic solidification model to explain Ge–Ni variations in iron meteorite chemical groups. *Geochim. Cosmochim. Acta* **46**, 259–268 (Abstract No. 5146).

Pearce N. J. G., Perkins W. T., Westgate J. A., Gorton M. P., Jackson S. E., Neal C. R. and Chenery S. P. (1997) A compilation of new and published major and trace element data for NIST SRM 610 and NIST SRM 612 glass reference materials. *Geostandard Newslett.* **21**, 115–144.

Raghavan V. (1988). *Phase Diagrams of Ternary Iron Alloys*, vol. 2. Indian National Scientific Documentation Centre, New Delhi, India, pp. 209–217.

Rasmussen K. L., Malvin D. J. and Wasson J. T. (1988) Trace element partitioning between taenite and kamacite–Relationship to the cooling rates of iron meteorites. *Meteoritics* **23**, 107–112.

Sellamuthu R. and Goldstein J. I. (1983) Experimental study of segregation in plane front solidification and its relevance to iron meteorite solidification. In *Proc. Lunar Planet. Sci. Conf. 14th. J. Geophys. Res.* **88**, B343–B352.

Sellamuthu R. and Goldstein J. I. (1984) Measurement and analysis of distribution coefficients in Fe–Ni alloys containing S and/or P—Part I: K_{Ni} and K_P. *Metall. Trans.* **15A**, 1677–1685.

Sellamuthu R. and Goldstein J. I. (1985) Analysis of segregation trends observed in iron meteorites using measured distribution coefficients. In *Proc. Lunar Planet. Sci. Conf. 15th. J. Geophys. Res.* **90**, C677–C688.

Ulff-Møller F. (1998) Effects of liquid immiscibility on trace element fractionation in magmatic iron meteorites: a case study of group IIIAB. *Meteorit. Planet. Sci.* **33**, 207–220.

Walker R. J., McDonough W. F., Honesto J., Chabot N. L., McCoy T. J., Ash R. D. and Bellucci J. J. (2008) Modeling fractional crystallization of Group IVB iron meteorites. *Geochim. Cosmochim. Acta* **72**, 2198–2216.

Wasson J. T. (1985) *Meteorites: Their Record of Early Solar-System History*. W.H. Freeman, New York.

Wasson J. T. (1999) Trapped melt in IIIAB irons: solid/liquid elemental partitioning during the fractionation of the IIIAB magma. *Geochim. Cosmochim. Acta* **63**, 2875–2889.

Wasson J. T. and Richardson J. W. (2001) Fractionation trends among IVA iron meteorites: contrasts with IIIAB trends. *Geochim. Cosmochim. Acta* **65**, 951–970.

Watson H. C., Watson E. B., McDonough W. F. and Ash R. D. (2005) Siderophile element profile measurements in iron meteorites using laser ablation ICP-MS. *Lunar and Planet. Sci. XXXVI.* Lunar and Planetary Institute, Houston (CD-ROM). #2141 (abstr.).

Watson H. C., Watson E. B., McDonough W. F. and Ash R., (2008) Low temperature siderophile element partition coefficients in iron meteorites. *Lunar and Planet. Sci. XXXIX.* Lunar and Planetary Institute, Houston (CD-ROM). #2374 (abstr.).

Willis J. and Goldstein J. I. (1982) The effects of C, P, and S on trace element partitioning during solidification in Fe–Ni alloys. In *Proceedings of the Lunar and Planetary Science Conference, 13th, Part I. J. Geophys. Res.* **87** (Suppl.), A435–A445.

Yang J. and Goldstein J. I. (2005) The formation mechanism of the Widmanstätten structure in meteorites. *Meteorit. Planet. Sci.* **40**, 239–253.

Associate editor: David Mittlefehldt